Sounding of subsurface concrete defects using frequency response of flexural vibration

S. Blaney[a,1,*], R. Gupta[b,2]

[a]*Dept. of Mech. Eng., University of Victoria, 3800 Finnerty Rd, Victoria, BC V8P 5C2, Canada*
[b]*Dept. of Civil Eng., University of Victoria, 3800 Finnerty Rd, Victoria, BC V8P 5C2, Canada*

Abstract

Standard sounding procedures such as hammer percussion and chain drag can be used to locate subsurface concrete defects, but are often subject to the individual judgement and ear of trained inspectors. However, defect depth information can be difficult to gauge by ear alone. By recording audio and analyzing the frequency content of sounding via hammer percussion, a single- and triple-link chain drag, and a novel speaker-based excitation procedure, simulated defects in concrete test slabs were detected. The speaker-based method shows the capacity to detect a similar number of defects as chain drag methods, though it is slightly less effective than the hammer method. The duration and type of the acoustic signal used by the speaker to induce vibration are important factors in performance of the speaker-based method. The detectability of a defect via all methods tested depended largely on the ratio of defect depth to defect lateral dimensions; defect detectability was shown to drop after this ratio exceeded about 0.35.

Keywords: Concrete, Defects, Sounding, Vibration methods

*Corresponding author
Email addresses: blaney@uvic.ca (S. Blaney), guptar@uvic.ca (R. Gupta)
[1]Graduate Student
[2]Associate Professor

1. Introduction

1.1. Problem Statement

Sounding of concrete via a variety of impactors including coins [1], steel spheres [2], hammers [3], and steel chain [4] has been shown to be capable of detecting defect locations. The depth of the defect can be estimated using a frequency analysis of the recorded contact or non-contact measurement of the response [1, 2, 5]. The work described herein assesses the relative performance of three readily-available impactors (hammer, chain, and speaker) in detecting voids and delaminations in concrete specimens. While hammer-based and chain-based excitation for concrete sounding are well established, speaker-based excitation for concrete sounding using microphones is unexplored. All three methods are low-cost, but the ability to accurately control and change the contact time between a speaker and the concrete surface it excites using different acoustic signals is a feature not available to hammer or chain-based methods (which require a new impactor of a different size altogether to change impact time).

1.2. Concrete Sounding Background

Several standard methods for sounding concrete to detect delaminations are outlined by ASTM D4580/D4580M – 12 [6], including a chain drag procedure, which may be performed with an actual chain dragged over the concrete surface or with hammer-based tapping. This standard specifies that the detection of delaminations occurs by the operator of the test noting dull or hollow sounds [6]. This procedure is subject to the ability of the operator to identify and make note of the sound of the defect-laden concrete. The depth of the defect can be difficult to detect by ear. A hammer percussion test may be said to be a type of coin tap test that uses a hammer as the impactor [7].

To remove the subjectivity of operator variance from the tests, the sound of the impact can be recorded by a microphone and the frequency content of the acoustic recording is used to identify defects. Sun, Zhu, and Ham [4] used a microphone to record the response of the concrete for a chain drag test [4]. A hammer percussion test using a microphone to record the sound of the impact has been shown by Wu and Siegel [3] to be roughly as effective as a contact force-based measurement of the vibration response in detecting problem areas in an aircraft skin specimen. Asano, Kamada, Kunieda, and Rokugo [5] demonstrated use of a microphone and digital audio card on concrete specimens. The use of a hammer sounding technique for Pavement

was demonstrated by Felicetti [8]. Cheng, Cheng, and Chiang [1] showed coin tapping recorded using a microphone could be used to detect voids in concrete specimens.

When excited by an impact, concrete of a plate-like shape will vibrate prominently in thickness and flexural modes [9]. Concrete defect detection by sounding uses the concept that waves travelling in the concrete are reflected at a planar air-concrete interface due to the low specific acoustic impedance of air. The impact-echo method takes advantage of this reflection of thickness mode vibration waves to detect voids [9]. For the sounding tests performed in this study, rather than measuring the vibration at the concrete surface as in the impact-echo method prescribed by ASTM C1383 – 15 [10], the concrete vibration is recorded via the reflected wave in the air in a manner similar to an air-coupled impact echo procedure such as the one described by Zhu and Popovics [11]. However, the methods of excitation used in this study (the hammer, chain, and speaker) produce contacts with the concrete specimens that have longer contact times in comparison to those involved in an air-coupled impact echo test. As longer contact times limit the maximum useful frequencies of the tests [12], flexural frequencies of vibration, which are lower than thickness mode vibration frequencies, should be the most prominent modes of vibration found in the audio recordings. That is, frequency peaks associated with the flexural modes of vibration will be the most prominent in the amplitude spectrum of the fast Fourier transform of the recorded acoustic signals.

Haya, Luo, and Uomoto [13] used an impact acoustic method coupled with wavelet analysis to observe the early part of the response signal to characterize defect strength and defect detection, and found the dominant frequency component over the total signal duration to characterize the boundary conditions or defects inside a specimen. Felicetti [8] observed a vibration of the impact device in the later part of the response signal recorded by the microphone, and used comparison of the frequency spectrums between damaged and undamaged pavement as a basis for defect detection. A similar but more cursory comparison forms the basis of defect detection in this work.

1.3. Expected flexural frequency peak

The relationship between the resonant frequency peaks associated with flexural vibration and the depth of a defect or thickness of a plate depend on the lateral size, shape, and boundary conditions of the plate [2]. In the case of acoustic sounds above the location of a planar void or delamination defect in

concrete, plate thickness is the depth of the defect. In this study, the actual concrete above the defects is restricted or damped along the bottom surface to some degree by the foam (in the case of simulated voids) or plastic (in the case of simulated delaminations). Approximation of boundary conditions in the theoretical treatment of the concrete above a simulated defect to simplify calculation of expected flexural frequency peaks was used by Cheng and Sansalone [2], with simply supported boundary conditions.

Given concrete properties, lateral dimensions, plate depth, the expected frequency of vibration can be computed using closed form solutions for vibrating plates or finite element analysis. The appropriate dimensions for the specimens used in this study are shown in Figure 1. The defect depth is shown as h, the lateral size of delaminations is shown as b, and the diameter of the voids is shown as $2a$.

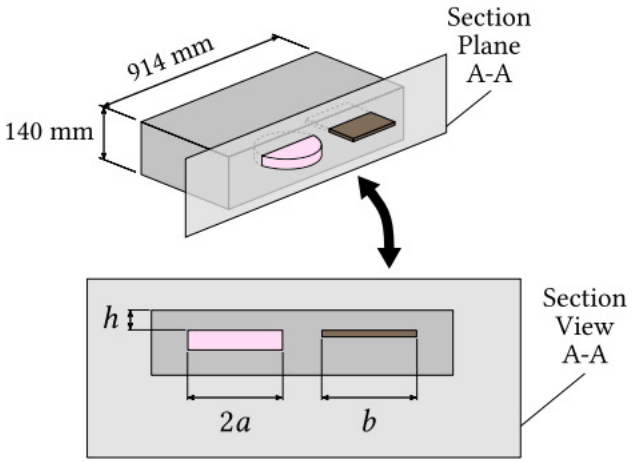

Figure 1: Slab defect depth and lateral size for voids (left) and delaminations (right).

Thus, the depth of a defect is the thickness of the plate of concrete that rests on top of a defect. Only the fundamental modes of vibration are considered. Impacts occur roughly over the center of defect locations, so fundamental frequencies should have the largest amplitude [2]. Higher modes of vibration are also likely to be recorded as the impact will likely not be perfectly centered. The equations used to relate the defect depth to the frequency for a thin square plate clamped on all sides are shown in a form similar to that of Leissa [14]:

$$\lambda = 2\pi f b^2 \sqrt{\frac{\rho h}{D}} \tag{1}$$

$$D = \frac{Eh^3}{12\,(1-\nu^2)} \tag{2}$$

In which λ is a dimensionless frequency parameter that depends on boundary conditions, mode of vibration, and plate thickness ratio, f is the frequency of vibration in Hz, b is the side length of the square plate in m, ρ is the mass density of the plate in kg/m^3, h is the thickness of the plate in m, D is the plate flexural rigidity in N·m, E is the dynamic elastic modulus in Pa, and ν is the Poisson's ratio. Leissa [14] offers a value of $\lambda = 35.998965$ for a thin plate only. A plot by Nelson [15] offers a range of normalized angular frequency ratios (ω/ω_0) as a function of thickness to side ratio (h/b) that can be used to obtain estimates of the expected frequencies for the range of plate thicknesses used in this study. This plot is shown in Figure 2.

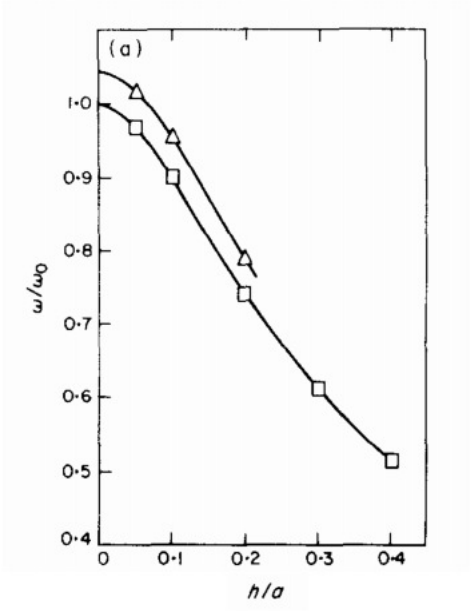

Figure 2: The plot used to estimate h/b from Nelson [15]: "Normalized frequency, ω/ω_0, as a function of thickness-side ratio for a square (C-C-C-C) plate. □, Present approximation; △ Cheung and Chakrabarti results. (a) m = 1, n = 1."[3]

[3]Reprinted from Journal of Sound and Vibration, Vol 60, H. M. Nelson, High frequency flexural vibration of thick rectangular bars and plates, pp 101–118, Copyright (1978), with permission from Elsevier

In the plot shown in Figure 2, the square-box "present approximation" is the curve used for all estimations of ω/ω_0. The angular frequency for a thin plate with $h/b = 0$ is ω_0, and the angular frequency at h/b up to 0.4 can be estimated. A frequency computed using Equation 1 must be multiplied by the appropriate ω/ω_0 ratio obtained using Figure 2 according to the h/b ratio. The h/a in Figure 2 is equivalent to h/b in the terminology used in this work.

The equations for circular plates are also presented in a form similar to that used by Hosseini-Hashemi, Es'haghi, Taher, and Fadaie [16]:

$$\beta = 2\pi f a^2 \sqrt{\frac{\rho h}{D}} \tag{3}$$

In which β is a dimensionless frequency parameter, and a is the circle radius in m. To obtain values for β, Hosseini-Hashemi, Es'haghi, Taher, and Fadaie [16] offer a host of values for clamped circular plates.

These equations can be used to compute either a defect depth given a measured frequency, or an expected frequency from a measured depth. In order to do so, knowledge of concrete material properties and the defect lateral defect dimensions is required. The dimensionless frequency parameters that originate from published closed-form solutions of vibrating plates are also required. While extensive sounding using a grid can estimate lateral dimension information, other non-destructive methods such infrared thermography offer a more expedient alternative.

2. Specimens

Seven reinforced concrete test slabs were constructed with simulated defects to evaluate the performance of several acoustic sounding methods. Six of the slabs, numbered 1 through 6, contained simulated voids and delaminations that were introduced during casting. The remaining slab served as a control slab that was free of induced defects or imperfections, numbered slab 7. All slabs are the same nominal size: 36 × 36 × 5.5 inches (approximately 914 × 914 × 140 mm). This ensures the lateral dimensions of the plate are more than six times the thickness, in accordance with the ASTM Standard C1383 – 15 [10] definition of a plate.

Each slab contains a grid of steel rebar reinforcement— three equally-spaced 800 mm lateral pieces of 10 mm diameter rebar ½ inch (12.7 mm)

from the bottom surface of the slab, and three equally-spaced 800 mm longitudinal pieces of rebar fastened directly on top of and perpendicular to the lateral pieces using bailing wire. This reinforcement simulates that typically observed in slab-on-grade reinforced concrete slabs. Small plastic rebar chairs support the bottom layer of rebar to maintain the ½ inch (12.7 mm) cover.

The concrete mix was supplied by Butler Brothers Supplies Ltd. of Saanichton BC. Nominal properties of the concrete mix are 32 MPa target strength, 75±20 mm slump, 6±1% air, with 20 mm maximum aggregate size. A slump test performed during casting yielded a measurement within the specified range. The concrete was left in the forms during the curing process with the upper surface exposed to ambient weather conditions. No moist curing was used at any time during the curing process. The ambient temperature during the first 28 days of curing ranged between roughly 9 and 29.7 °C. Several 100 mm diameter 200 mm height test cylinders were cast at the same time as the slabs and left next to the slabs to expose the cylinders to curing conditions similar those experienced by the slabs. These cylinders were used to estimate the density and compressive strength of the concrete slab specimens. Tests were performed on the cylinders 80 days after casting to allow full curing of the cylinders under ambient conditions. The concrete density of the cylinders was roughly 2300 kg/m^3 and the mean of three tested specimens resulted in a compressive strength of 23.6 MPa.

The essential dimensions of the control slab are shown in Figure 3a, including reinforcement (reinforcement is the same for all slabs). An example of the nominal configuration of a slab with defects is shown in Figure 3b, which illustrates the key parameters of slab 3, including the simulated voids. Other simulated defect slabs have a similar configuration with different nominal defect locations. The as-built simulated defect locations show some variance from the nominal configurations.

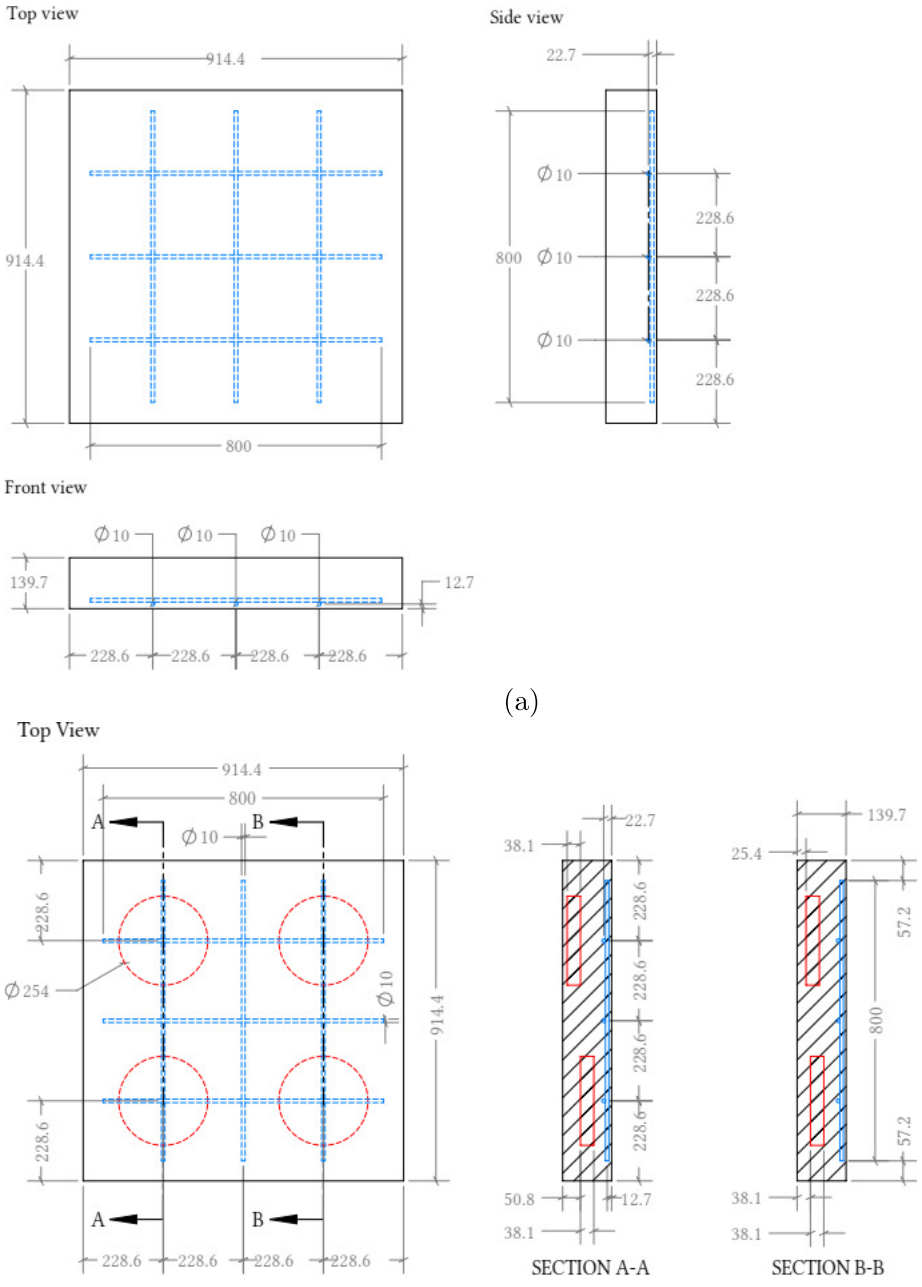

Figure 3: All dimensions are in mm: (a) Dimensions of the control slab; (b) Dimensions of slab 3 including nominal void locations (red) and rebar (blue).

Artificial voids and delaminations were deliberately introduced in slabs 1 through 6. Each slab contains a different arrangement of circular foam discs replicating voids or square plastic sheets simulating delaminations. Foam discs and plastic sheets have previously been used by Lu [17] as well as Zhu and Popovics [11] to simulate voids and delaminations, respectively. The void-simulating discs are cut from 1.5 in (38.1 mm) thick polystyrene insulation foam. The simulated delamination plastic squares are constructed of three layers of HDPE plastic laminated at the edges using an adhesive cloth tape, and are roughly 9 mm thick overall. Foam discs and plastic sheets are shown in Figure 4a and 4b.

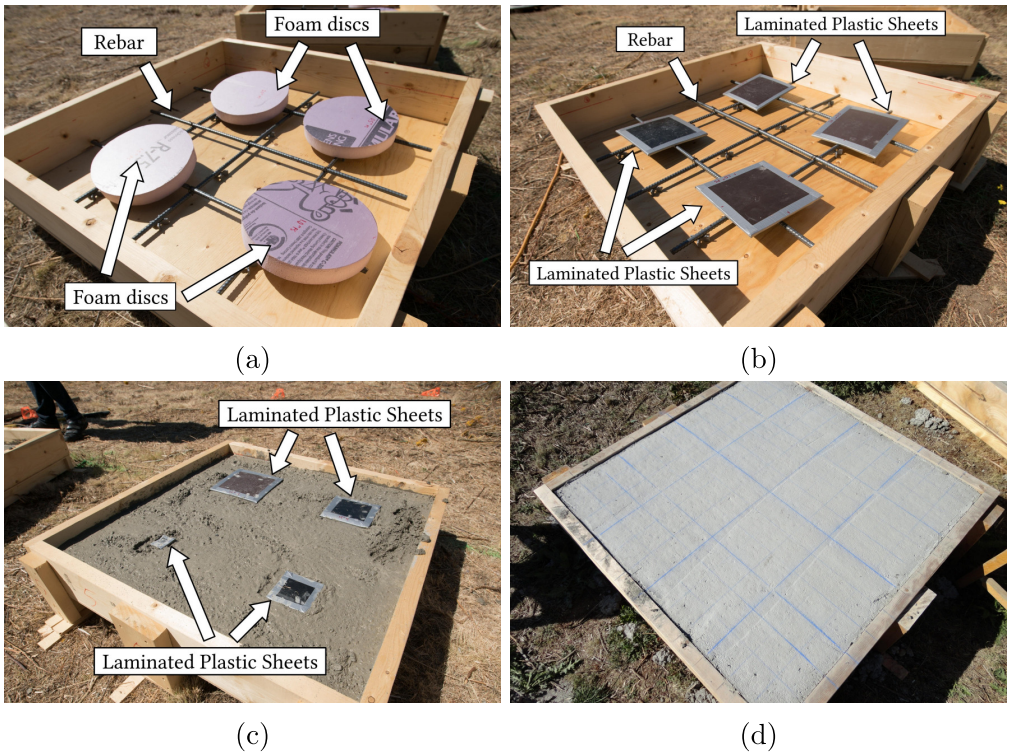

Figure 4: (a) Formwork showing the foam discs used to simulate voids; (b) Formwork with laminated plastic sheets used to simulate delaminations; (c) In-situ placement of laminated plastic sheets during casting; (d) Slab shown in formwork with 3 × 3 in surface grid shown.

The lateral defect dimensions (width and length for delaminations and diameter for voids) as well as the nominal depth of the simulated defects

(distance from the upper concrete surface to the top surface of the foam or plastic) are different for each slab. Simulated defects were placed with the surface of the plastic or foam parallel to the top and bottom of the slab. The center of each simulated defect surface was placed roughly 9 in (229 mm) from the two nearest edges of the slab. The plastic and foam were hand placed in the slab during casting without the aid of any anchoring system, as shown in Figure 4c. As a result, some significant variation in the nominal and actual simulated defect location was observed. The as-built lateral location of the simulated defects was confirmed for reference using infrared thermography. Actual as-built depths were measured after acoustic testing by drilling the slabs and measuring the depth to the nearest millimeter using ruled calipers. For defects that were left slightly out-of-plane (defects that did not have perfectly uniform depth), multiple measurements were taken and the mean was computed, as necessary. A summary of all as-built simulated defect dimensions and depths is included in Table 1. Expected frequencies calculated based on as-built locations using Equations 1, 2, and 3 are presented in Table 1 along with those measured via hammer-based accelerometer testing for defects that are detected.

Table 1: As-built and target dimensions and depths of defects of voids and delaminations (Del). Expected and measured frequencies are also presented.

No.	Type	Lateral Size (mm)	Target Depth (mm)	As-built Depth (mm)	Expected Freq. (kHz)	Accelerometer-measured Freq. (kHz)
1	Del	203×203	13	39	3.5	2.5
2	Del	203×203	25	49	4.3	3.2
3	Del	203×203	38	73	—	—
4	Del	203×203	51	82	—	—
5	Del	203×203	64	84	—	—
6	Del	203×203	76	101	—	—
7	Del	203×203	89	98	—	—
8	Void	⌀ 254	13	15	1.2	1.2
9	Void	⌀ 254	25	27	2.0	2.1
10	Void	⌀ 254	38	43	2.8	2.9
11	Void	⌀ 254	51	53	3.3	3.0
12	Void	⌀ 254	64	60	3.5	3.2
13	Void	⌀ 254	76	73	—	—
14	Void	⌀ 254	89	90	—	—
15	Del	203×203	38	62	4.7	4.0
16	Del	152×152	38	48	6.4	4.9
17	Del	102×102	38	84	—	—
18	Del	51×51	38	92	—	—
19	Void	⌀ 254	38	27	2.0	1.9
20	Void	⌀ 203	38	28	3.0	2.7
21	Void	⌀ 152	38	28	5.0	4.6
22	Void	⌀ 102	38	42	—	—

For the purposes of Table 1, defects are numbered starting in the upper left hand corner of each slab in a clockwise fashion, starting from the number one above the highest of the previous slab, as shown in Figure 5.

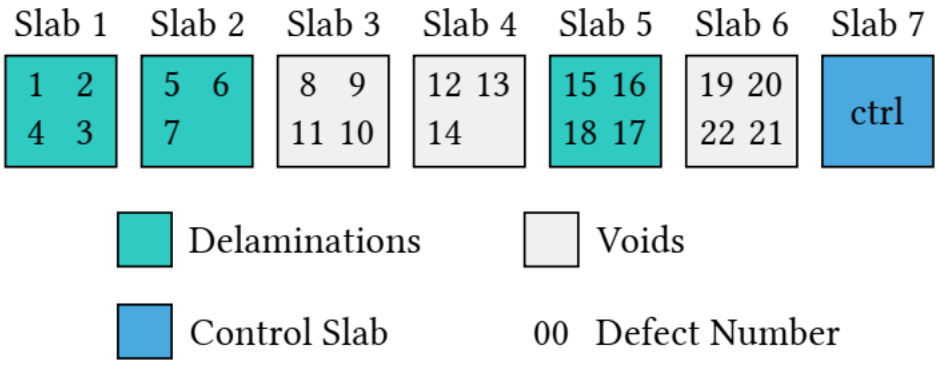

Figure 5: Defect numbering schemes for Table 1.

The top surfaces of the slabs are coarsely finished, resulting in exact as-built slab thickness to vary from the nominal 140 mm by roughly plus or minus 7 mm. All slabs and formwork are approximately level. A 3 × 3 in (76 mm) rectilinear grid, as shown in Figure 4d was established on the slab surfaces during testing to ensure consistent excitation location. The slabs were removed from formwork for acoustic testing, with two opposite edges resting on dimension lumber that was on a soft dirt foundation. There was no more than 3.5 in (89 mm) overlap between the wooden support and the bottom of a slab at the edge.

3. Methods

3.1. Audio recording and processing

Audio recording was performed using a Zoom H1 digital voice recorder. The Zoom H1 can record at a sample rate of 96 kHz at 24 bit depth, which means a frequency response as high as 48 kHz can be observed in a recording. The Zoom H1 does analog-digital and digital-analog conversion at 24-bit depth, and signal processing at 32-bit to ensure no information is lost in the recording process.

The microphone used during all recording was a Polsen OLM-20 Dual Omnidirectional Lavalier Microphone. This microphone records two mono signals from two microphones, so only the left signal was used in this work. It has a specified flat frequency response from 30 Hz to 18 kHz, which is an acceptable range for the type of defects and analysis used in this study. The recorder and microphones are shown in Figure 6.

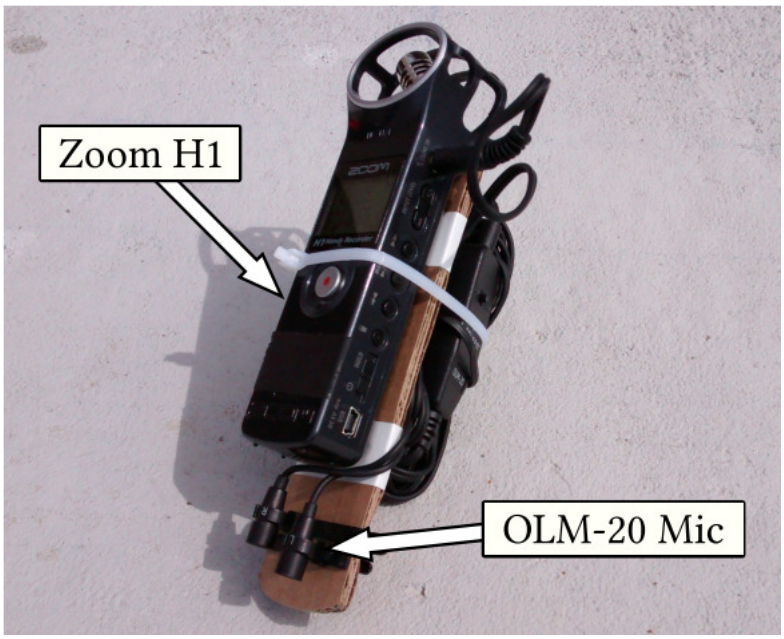

Figure 6: Microphone configuration showing two microphones and Zoom H1 recorder.

The Zoom H1 records the audio files in WAV format. Audacity® audio software was used to isolate the audio associated with a particular trial, which are then saved to shorter WAV files. Each of these short WAV files contains audio related only to a particular trial. Each file corresponds to a particular test case at a specific location over a simulated defect on a given slab. For example, one such file contains the audio of the hammer percussion test performed over the location of the shallowest defect of slab 3, and another file contains the same information but for the second shallowest defect. MATLAB® was used to extract frequency information out of the short WAV files. A single-sided fast Fourier transform (FFT) was generated for each trial, and the frequencies of the peaks of the amplitude spectrum are identified and recorded.

3.2. Hammer percussion sounding

Exact requirements for a hammer percussion sounding test are not well established by current sounding procedures such as those in ASTM standard D4580/D4580M – 12 [6]. However, the operating concept behind a hammer percussion test is similar to those tests and is relatively straightforward; a hammer is used by the operator to strike the concrete specimen, and the

resulting acoustic disturbance is used to garner information about the concrete specimen. Instead of listening to the response by ear, the audio signals were digitally recorded and processed as described in the preceding section to extract meaningful frequency information. The hammer strike locations on the slabs are nodes in the 3 × 3 inch surface grid roughly over the center of each simulated defect (9 in from each of the two closest edges).

Figure 7: (Left to right) The 1, 2, 4, and 8 oz. hammers and Zoom H1 with OLM-20 mic. An 18 in (45 cm) ruler is shown for scale.

The four hammers were used in this study are shown in Figure 7. Three ball-peen hammers with weights 1, 2, and 4 oz. (0.028, 0.057, 0.113 kg, respectively) were used along with an an 8 oz. (0.227 kg) flat-head hammer. The diameters of the roughly hemispherical ball-peen hammers are 8.9 mm, 11.2 mm, and 17.4 mm for the 1, 2, and 4 oz. hammers respectively. According to the methods of Sansalone and Streett [18], steel ball impactors with diameters 8.9, 11.2, and 17.4 mm should have maximum excitation frequencies of 32.7, 26.0, and 19.8 kHz respectively. However, a hammer head has a noticeably higher mass in comparison with a steel ball of the same diameter as the hammer head. The mass to contact stiffness ratio determines the contact time for an impactor. Accordingly, the steel ball-peen hammers have higher contact times and lower maximum excitation frequencies than steel balls of the same diameter. The microphone was hand-held at a lateral distance of 56 mm or less from the impact location: less than 40 % of the slab thickness as in an air-coupled impact echo test [11]. The configuration

of the hammer impact test is shown in Figure 8.

Figure 8: Hammer percussion test configuration.

3.3. Speaker-based excitation sounding

A novel sounding procedure used a speaker (electroacoustic transducer) and the same operating concept as the hammer percussion method: a concrete specimen is vibrated and the audio response is recorded and processed. Gudmarsson, Ryden, and Birgisson [19] have shown a speaker is capable of non-contact resonance frequency excitation in asphalt concrete, but used an accelerometer on the surface for measurements. To adapt a speaker for use with sounding, the speaker excitation was made via contact, and the recording was performed using the same microphone procedure as the hammer percussion test. A speaker was temporarily affixed via an adhesive pad to the concrete specimen surface directly above the center of a defect location and variety of signals were played by the speaker to excite the concrete specimen.

There were a total of sixteen signals tested, including half-sinusoid "bump" features and symmetric up-down ramp functions in the image of a "spike" of durations 0.5, 0.2, and 0.1 milliseconds. The remaining ten signals were logarithmic chirps of varying length. Up-chirps started at an instantaneous frequency of 100 Hz and ended at 8 kHz, while down-chirps progressed oppositely from 8 kHz to 100 Hz. Chirp lengths of 8, 20, 200, 1000, and 2000 ms were used.

The setup for the speaker-based excitation test is shown in Figure 9. The locations of the speaker on the surface of the concrete specimen are the same as those struck by the hammer during percussion sounding. A Boombx V1 vibration speaker with a frequency response range from about 0.3 to 10 kHz was used for all speaker excitation. The speaker unit is detachable and connects to the power box of the system using a 3.5 mm audio cable. The excitation signals were played from a computer using Audacity® and a Syba AUD201 USB soundcard.

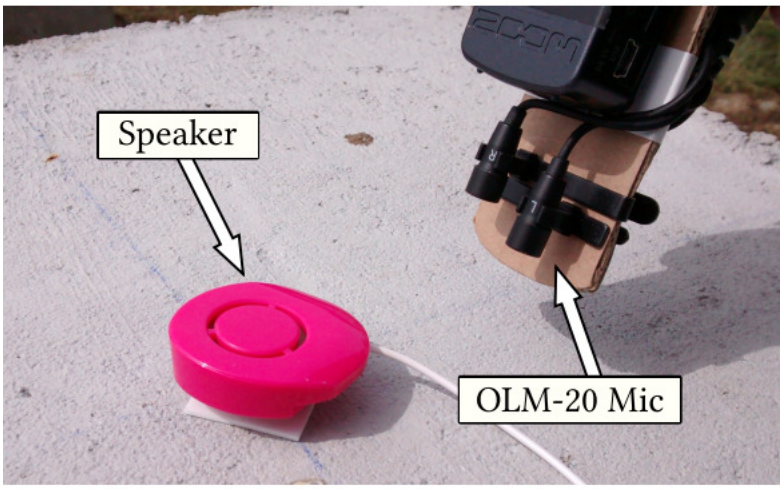

Figure 9: Close-up view of speaker unit attachment to slab surface.

3.4. Modified chain drag

The chain drag is a well-established test procedure for detecting delaminations in concrete bridge decks as in ASTM standard D4580/D4580M – 12 [6]. In practice, a chain drag is performed by an operator who drags a chain over a concrete deck or floor and listens for problem areas, which are marked with paint when detected. For this study, a three-link chain was dragged over the slab surfaces above where defects are located. The chain used was a hot dipped galvanized proof coil chain with link diameter 3/8 inch (9.5 mm) and total link length 2 1/8 in (54 mm). However, it has been reported that multiple chain links used during the standard test can sometimes produce unwanted noise and false positives in part due to the added noise of chain links bumping into each other [4]. With self-noise due to chain links colliding with each other in mind, a single-link chain drag was also performed, in

addition to the three link drag. A contraption was designed and constructed in which the chain is attached via a wire and foam connector to a 39 inch (991 mm) aluminum tube. The foam prevents unwanted noise from collisions between the aluminum tube and the chain link. The Zoom H1 recorder and microphones are mounted to the aluminum pole to give better acoustic access to the source of the sound signal, as shown in Figure 10.

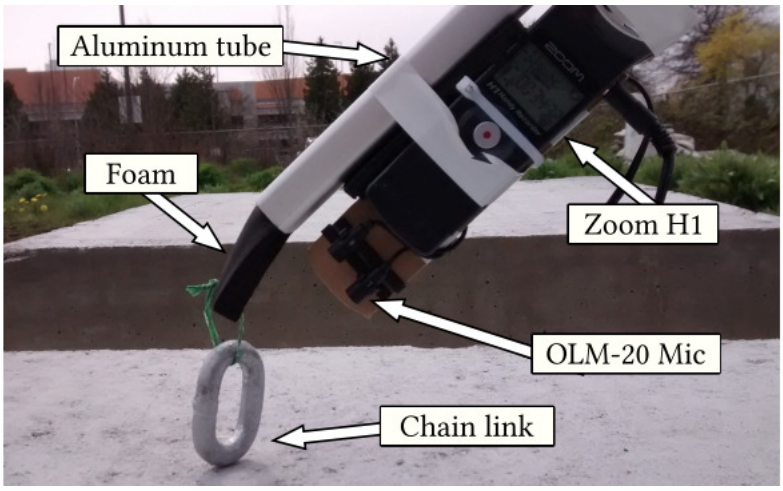

Figure 10: The single-link chain drag test configuration during a pass over a test slab.

3.5. Accelerometer and glass disc reference measurements

To validate the hammer data against a reliable reference measurement, accelerometer data was also recorded for hammer tests. As shown in Figure 11 An acclerometer was placed at 2 in (51 mm) or less lateral distance from the impact location for all tests and the response was recorded to offer reliable baseline data for hammer performance. An Olson Instruments RTG-1 Resonance Test Gauge (which uses a PCB Piezotronics 353B15 accelerometer) was used as the system for all accelerometer tests. The chain and speaker methods used did not produce impacts of the magnitude required by the RTG-1 system, so accelerometer data was recorded only for the hammer tests.

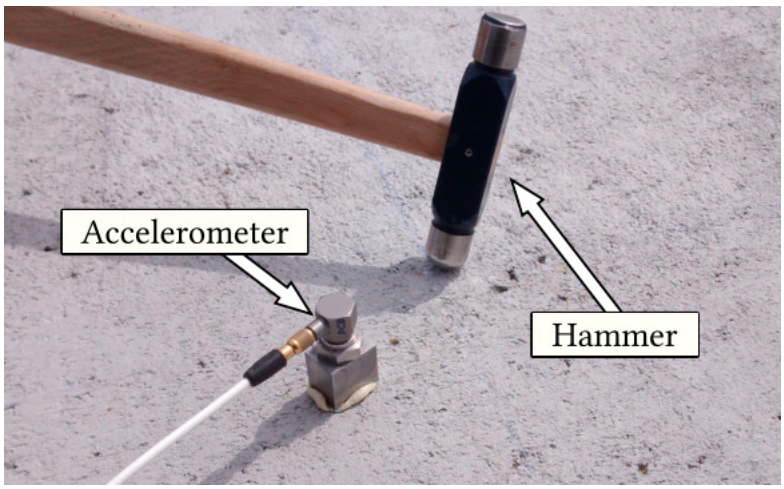

Figure 11: Accelerometer configuration for hammer impact test on concrete.

The V1 speaker performance was evaluated using a glass disc. The speaker was placed in the center of a glass disc and the response to the same battery of signals used with the concrete was recorded. The glass disc (with diameter 500 mm and thickness 5.8 mm) was placed on acoustic foam with a circle cutout so that only the outer 1 in (25 mm) of the disc rested on the foam. With this method of support, the plate can be considered to have roughly free boundary conditions. By testing the speaker on another medium with more well-known dimensions and boundary conditions like the glass disc, the features of the acoustic response caused by the speaker itself can be distinguished from those caused by the concrete vibration. A hammer test with both microphone recording and a contact accelerometer was also performed on the glass to verify the frequency peaks observed in the speaker test.

4. Defect detection performance

The basis for the detection of a defect is a comparison between the frequency spectrum of a test on a slab location to the frequency spectrum recorded at a similar place on the control slab. While the most prominent peak in the frequency spectrum is an important consideration in this comparison, the size and location of other peaks is also of interest. For example, in the hammer test results, defects that are not detected may have different prominences in peaks compared to the control slab. However, they typically

demonstrated low frequency peaks in the vicinity of 400 Hz and 700 Hz, as well as a higher frequency peak between 12 and 15 kHz. The lower peaks are to be expected from the flexural vibration of the entire slab, and the higher peaks are possibly caused by compressive vibration of the slab (of the type exploited by impact echo methods). The exact forms of the response signals for defects and the control slab depended on excitation methods (hammer, speaker, or chain) and parameters (impactor size, mass, or excitation signal).

A comparison of the frequency spectrum for defects that are detected and another that is not, along with the frequency spectrum of the control slab is shown in Figure 12 for the 2 oz. hammer test, as recorded using the Zoom H1. The spectrums have been normalized by their maximum value for the purposes of Figure 12 as the varying absolute amplitudes of the different spectrums make the comparison visually difficult otherwise. Similarly, the frequency in Figure 12 has been limited from 0 to 7 kHz to frame the peaks of interest appropriately.

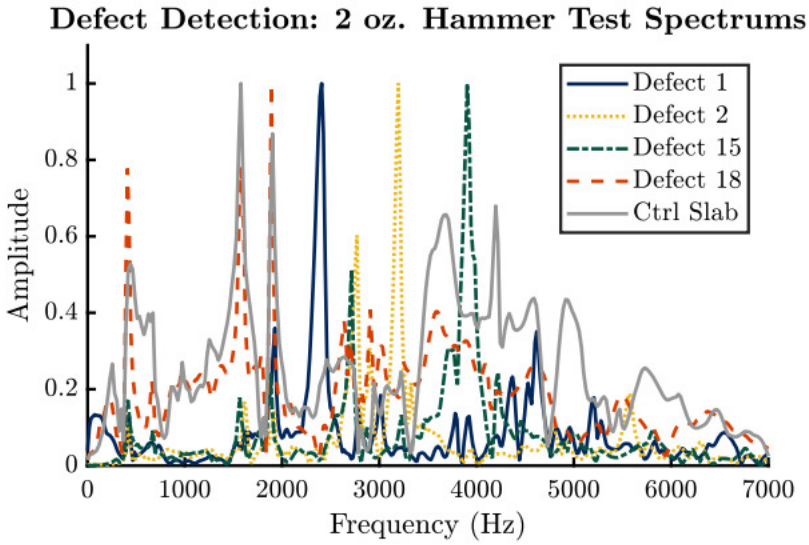

Figure 12: Frequency spectrums for 2 oz. hammer test showing detected and undetected defects spectrums along with the control slab spectrum.

The frequency spectrums for Defects 1, 2, and 15 in Figure 12 have a most prominent peak that indicates a dominant flexural mode of vibration, and stand in stark contrast to the shape and form of the control slab frequency spectrum. Less prominent peaks in these spectrums may correspond to other

modes of vibration or overtones. Importantly, the most prominent peaks in these three microphone-recorded spectrums have a mean percent difference of 5 % from those measured using the contact accelerometer. Deeper defects and those with smaller lateral size have higher frequency peaks than shallower defects with larger lateral size. Spectrums from the other hammers show the same trends as those in the 2 oz. hammer test.

Conversely, the frequency spectrum for Defect 18 shown in Figure 12 has significant similarity to the control slab spectrum. There are peaks near 400 Hz, 1.6 kHz, and 1.9 kHz, and there is no other dominant peak to indicate the kind of flexural vibration associated with a subsurface defect. A comparison between the frequency spectrum for Defect 18 and the control slab is not adequate to say that a defect has been detected.

A summary of the defect detection via each of the three primary method tested is shown in Table 2. For the hammer and speaker tests, if one variation detected the defect, the result in Table 2 is a positive detection. For example, if only two of the six chirps tested detect a defect, the result in Table 2 is considered a positive detection for that defect for the speaker chirp method. Out of 22 total defects, the hammer methods detected 12 defects, the speaker methods detected 9 defects, and the chain drag methods detected 10 defects.

Table 2: Defects detected by the sounding methods used in this study.

Detected: yes (Y) or no (—)						
	Hammer		**Speaker**		**Chain Drag**	
Defect No.	Acoustic	Accel.	Bumps /Spikes	Chirps	Single-link	Triple-link
1	Y	Y	Y	Y	Y	Y
2	Y	Y	Y	—	—	Y
3	—	—	—	—	—	—
4	—	—	—	—	—	—
5	—	—	—	—	—	—
6	—	—	—	—	—	—
7	—	—	—	—	—	—
8	Y	Y	Y	Y	Y	Y
9	Y	Y	Y	Y	Y	Y
10	Y	Y	—	Y	Y	Y
11	Y	Y	—	—	Y	Y
12	Y	Y	—	—	—	Y
13	—	—	—	—	—	—
14	—	—	—	—	—	—
15	Y	Y	—	Y	—	—
16	Y	Y	—	Y	—	—
17	—	—	—	—	—	—
18	—	—	—	—	—	—
19	Y	Y	Y	Y	Y	Y
20	Y	Y	Y	Y	Y	Y
21	Y	Y	—	—	Y	Y
22	—	—	—	—	—	—

4.1. Slab vibration and thickness ratio

Table 3 summarizes defect detection based on detection method and plate thickness using the ratio of depth to side length for delaminations) and the ratio of depth to diameter for voids (h/b and $h/2a$ respectively).

Table 3: Defect detection for each method sorted by defect depth to lateral size ratio.

Defect			**Detected: yes (Y) or no (—)**		
No.	Type	h/b or $h/2a$	Hammer	Speaker	Chain
8	Void	0.06	Y	Y	Y
19	Delam	0.11	Y	Y	Y
9	Void	0.11	Y	Y	Y
20	Void	0.14	Y	Y	Y
10	Void	0.17	Y	Y	Y
21	Void	0.18	Y	—	Y
1	Delam	0.19	Y	Y	Y
11	Void	0.21	Y	—	Y
12	Void	0.24	Y	—	Y
2	Delam	0.24	Y	Y	Y
13	Void	0.29	—	—	—
15	Delam	0.31	Y	Y	—
16	Delam	0.32	Y	Y	—
14	Void	0.35	—	—	—
3	Delam	0.36	—	—	—
4	Delam	0.40	—	—	—
22	Void	0.41	—	—	—
5	Delam	0.41	—	—	—
7	Delam	0.48	—	—	—
6	Delam	0.50	—	—	—
17	Delam	0.82	—	—	—
18	Delam	1.80	—	—	—

As Table 3 shows, there appears to be a relationship between the detectability of a defect via the sounding methods used and the thickness of the plate of concrete left above the defect. Values in Table 3 are sorted according to h/b or $h/2a$ as this measure is dimensionless. Although more data is required to accurately estimate the depth to side ratio cut-off point, the values in Table 3 seem to indicate that an h/b or $h/2a$ of about 0.35 or less seems to yield an acceptable level of detection.

If a defect is both deep and lacks sufficient lateral size, the vibration of the concrete above is no longer adequately plate-like and the vibration of

the slab as a whole appears to dominate the audio recording of the test. So, for a square defect such as a delamination with side length 8 in (203 mm), detection would be expected up to depths of about 2 in (51 mm). It is possible that the boundary conditions on an actual structure such as a bridge deck play a role in what ratio of depth to lateral size is acceptable.

4.2. Speaker performance: glass

The speaker tests on the glass plate offer insight into the speaker results for the concrete slabs. The plate is excited by the speaker in the center, which should excite modes of vibration with zero nodal diameters. The first four modes of vibration with zero nodal diameters can be computed using Equation 3. Required are the dimensions of the glass plate ($a = 0.025$ m, h = 0.0058 m), nominal glass material properties ($\nu = 0.24$, $E = 69$ GPa, $\rho = 2500\,\mathrm{kg/m^3}$), and the appropriate frequency parameters for a free circular plate from Leissa [14]. Computing the frequencies using these values yields $f_{01} = 205$ Hz, $f_{02} = 885$ Hz, $f_{03} = 2.02$ kHz, and $f_{04} = 3.62$ kHz where the first subscript indicates the number of nodal diameters and the second indicates the number of circular nodes in the vibration.

The first four prominent frequency peaks in the spectrum from the speaker test of the glass disc occur at 207 Hz, 879 Hz, 2.01 kHz, and 2.7 kHz. The first three are in near perfect agreement with the predicted peaks, although the fourth is not. A closer inspection reveals that a peak at roughly 3.6 kHz does exist, but the peak at about 2.7 kHz is more prominent. This is a likely indication that the speaker itself may be responsible for some peaks in close proximity to 2.7 kHz.

Comparison of the speaker data to the accelerometer and speaker data collected during a hammer test of the glass plate also supports the notion of speaker noise causing peaks. For the accelerometer hammer measurement the fourth peak is located at 3.74 kHz and for the hammer acoustic measurement the peak is located at 3.54 kHz; both are near the expected location of 3.62 kHz.

Up-chirp speaker signals appear to generate some kind of noise peaks in neighborhood 5.6 and 8.0 kHz. These peaks become more pronounced as the length of the up-chirp increases. Figure 13 shows frequency spectrums for down chirps for the glass disc showing the peaks associated with first four modes of vibration with zero nodal diameters.

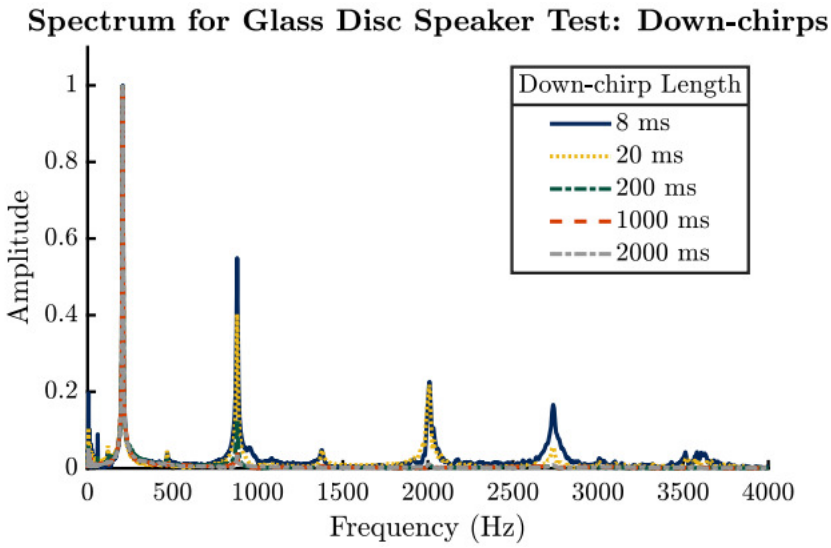

Figure 13: Normalized down-chirp spectrums for the glass speaker test showing peaks associated with modes of vibration with no nodal diameters.

Amplitudes in Figures 13 and 14 are normalized by the largest value in each spectrum to make the plots easier to view (the amplitude is also plotted on a logarithmic scale in Figure 14 for this purpose). Figure 14 shows a comparison of the 1000 ms up- and down-chirp signals for the glass disc. From Figure 14, it can be observed that the noise in the vicinity of 5.6 kHz can be found in both the up-chirp and down-chirp signals. The noise in the neighborhood of 8.0 kHz appears to be exclusive to the up-chirp signal.

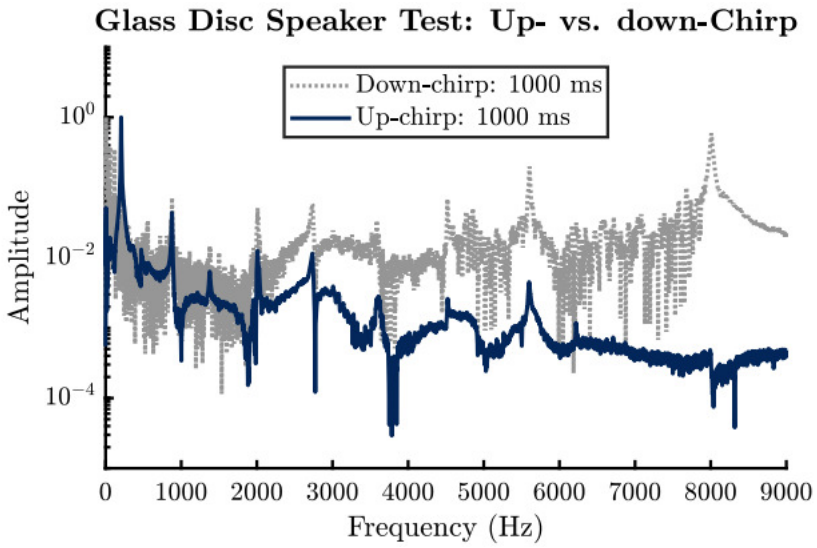

Figure 14: Comparison of normalized 1000 ms up- and down-chirp spectrums for the glass disc speaker test.

4.3. Speaker performance: concrete

The speaker performance for concrete is somewhat similar to that of the glass plate tests. In general, both impact-like speaker signals (half-sinusoid "bumps" or up-down ramp "spikes") and down-chirps generate peaks that appear to correspond to flexural vibration above defects, while the up-chirps produce more noise. While the glass disc testing indicates that these peaks are caused by the speaker itself, it is possible that this is a problem isolated to the specific speaker used in this work.

For impact signals, longer signals produced less noise but were limited in detection of defects that exhibited higher resonant frequencies. For example, normalized frequency spectrums for the signals tested above defect #8 are shown in Figure 15. To avoid interference from the frequency content of the excitation signal itself, all audio for the speaker is carefully selected to use only the part of the overall signal that corresponds to the response that follows the excitation signal.

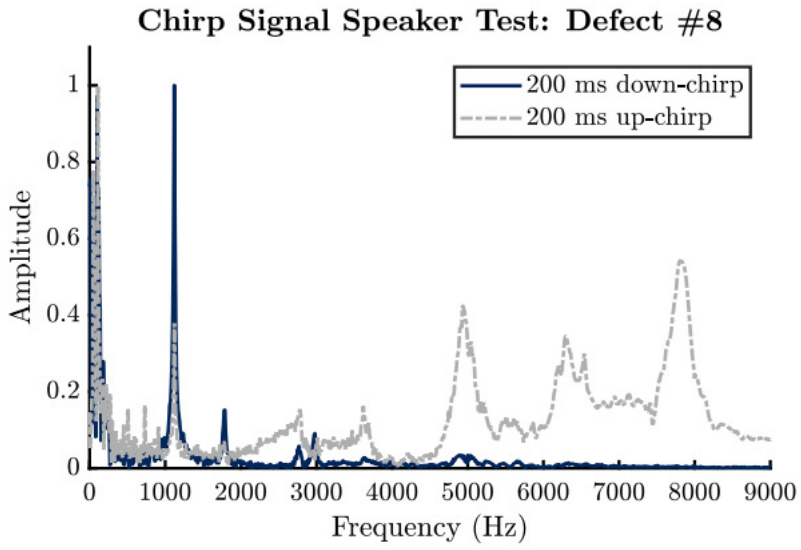

(a)

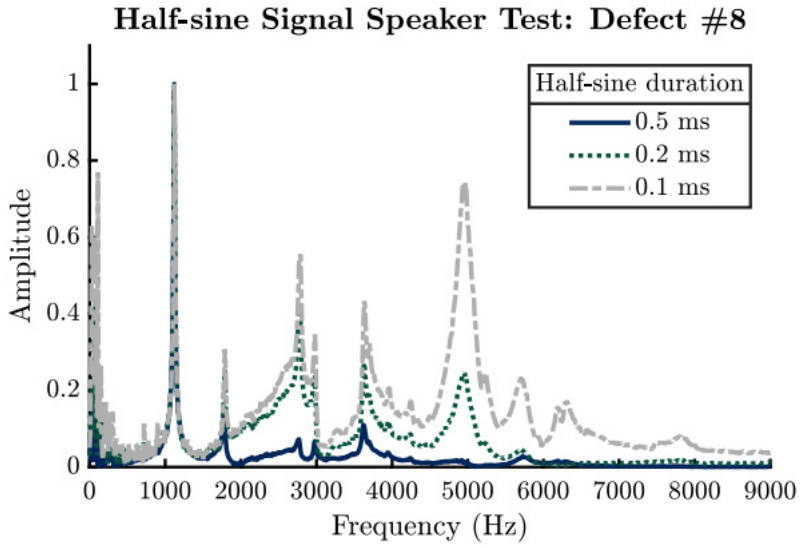

(b)

Figure 15: Frequency x-axis ranges are set to best display features of interest. (a) Comparison of normalized 200 ms up- and down-chirp spectrums for the concrete speaker test of defect #8. (b) Comparison of normalized spectrums for half-sine "bump" signals of different lengths for speaker test of defect #8.

As shown in Figure 15, there is a clear resonance peak that indicates defect detection at roughly 1120 Hz and other peaks that may be caused by

noise, other modes of vibration, or overtones. Up-chirps of longer duration like the 200 ms signal spectrums shown have significant noise in the 5–6 and 8 kHz range as was observed in the glass disc test. The noise in the 5–6 kHz range also appears in the spectrums for the shorter duration half-sine signals. The speaker used is very inexpensive and has a thin injection molded plastic casing. It is possible that this particular signal and duration produce some vibration of this speaker casing that causes the noise observed, but more investigation is required to determine the exact cause of these noise peaks with certainty. The low frequency noise (below about 300 Hz) appears to be at least somewhat related to the ambient conditions (primarily wind and nearby traffic and construction). The low frequency of this noise is not in a range that would be associated with concrete specimens and type of vibration explored in this study.

For chirps, as excitation signal length is increased, the impact of noise becomes more significant. The frequency spectrums for up-chirps indicate significantly more noise in the signal that those for down-chirps. Though no bias caused by transient vibrations is discernible, it may be difficult to detect due to frequency components from noise (likely attributable to ambient noise or speaker self-noise), which is evident to some degree in nearly all frequency spectrums for chirp-based tests. The frequency peaks in the spectrums for chirp based tests are consistent between chirp signals of different lengths, and betwen up- and down-chirps, but the relative magnitudes of the peaks fluctuate. For those defects detected by the chirp-based speaker test, the shorter signal lengths produce resonance peaks that have greater prominence compared to peaks attributed to noise or peaks that also appear in the control slab (that is, frequency peaks associated with non-defect vibration). To determine an optimal shape of the acoustic signal which produces minimal levels of noise and avoids transient vibration bias, testing with a larger variety of signal lengths is suggested. Of the chirp signals used in this work, the 8 ms down-chirp produced the least noise and most prominent resonance peaks.

4.4. Performance of hammer percussion and chain drag

The hammers used all demonstrated adequate sounding performance. The frequency spectrums of the hammers are generally very similar, but some variation between hammers is observable. The acoustic hammer tests were verified using a contact accelerometer. In general, the results of the accelerometer and acoustic tests are in very good agreement for the defects that are detected. The percent error between the accelerometer and hammer

measurements in this case is usually less than 5 % and always less than 12 %.

In general, for spectrums in which subsurface defects are detected there is very little difference between the frequency of peaks for different hammers (5 % difference or less). The peak that is most prominent may differ between hammers, but the frequencies of the peaks are generally very consistent between hammers provided a defect is detected. In order for the chain drag to produce meaningful results, the frequency peaks caused by noise from the chain links themselves needs to be removed from consideration. The chain links produce minor noise across a wide frequency range, but the most prominent noise occurs between 13 and 14.5 kHz. This noise occurs in both single-link and triple-link tests, indicating it is possibly cause by a vibration in the link itself. The prominence of the noise peaks in this range can be so large that it becomes difficult to properly detect peaks associated with defective concrete vibration in the frequency range of those expected in this study (about 1 to 12 kHz). Thus, the chain link frequency range for peak detection was deliberately limited to between 200 Hz and 13 kHz to avoid some self-noise from the chain. Since the exact frequency of the chain self-noise is likely dependent upon the chain properties, it may be advisable to verify chain noise parameters before conducting concrete sounding via a chain drag method with a particular chain.

5. Conclusions

This work evaluates the performance of three sounding methods in detecting simulated subsurface concrete defects in a series of test slabs. Hammer percussion, a speaker excitation method, and chain drags, were adapted as concrete sounding techniques for use with a microphone and recorder coupled with an audio file analysis procedure. The hammer percussion, speaker, and chain drag methods all detect a similar number of defects. In general, the ratio of depth of the concrete above a simulated defect to the lateral dimensions of the defect may be said to limit the detectability of the defect using the sounding methods. The speaker test was found to be sensitive to the length and type of the excitation signal. Speaker excitation signals with shorter durations produced more distinct results than longer signals in some cases, but more investigation is required to determine the exact effect of signal duration and type on frequency excitation and subsequent defect detection. Three chain links in series detected a larger number of defects

compared to a single chain link. Self-noise from the chain was observed but did not overlap with meaningful flexural frequency content associated with concrete defects for the slabs tested. More work is required to assess the relationship, if any, between the accuracy of depth estimation using frequency of flexural vibration and defect depth to lateral size ratio.

Acknowledgements

The authors would like to acknowledge the assistance of the fine technical support staff with the UVic Facility for Innovative Materials and Infrastructure Monitoring in constructing the test specimens. This work has been completed with financial support from India-Canada-IMPACTS and Networks of Centres of Excellence of Canada. In-kind support from Butler Brothers Supplied Ltd. is also acknowledged.

[1] C.-C. Cheng, T.-M. Cheng, C.-H. Chiang, Defect detection of concrete structures using both infrared thermography and elastic waves, Automation in Construction 18 (1) (2008) 87 – 92. doi:10.1016/j.autcon.2008.05.004.
URL http://www.sciencedirect.com/science/article/pii/S0926580508000812

[2] C. Cheng, M. Sansalone, The impact-echo response of concrete plates containing delaminations: numerical, experimental and field studies, Materials and Structures 26 (5) (1993) 274–285. doi:10.1007/bf02472949.
URL https://doi.org/10.1007/bf02472949

[3] H. Wu, M. Siegel, Correlation of accelerometer and microphone data in the "coin tap test", IEEE Transactions on Instrumentation and Measurement 49 (3) (2000) 493–497. doi:10.1109/19.850382.

[4] H. Sun, J. Zhu, S. Ham, Acoustic evaluation of concrete delaminations using ball-chain impact excitation, The Journal of the Acoustical Society of America 141 (5) (2017) EL477–EL481. doi:10.1121/1.4983343.
URL http://dx.doi.org/10.1121/1.4983343

[5] M. Asano, T. Kamada, M. Kunieda, K. Rokugo, I. Kodama, Impact acoustics methods for defect evaluation in concrete, in: Proceedings

International Symposium Non-Destructive Testing in Civil Engineering (NDT-CE), Berlin, 2003.

[6] ASTM D4580 / D4580m-12, Standard Practice for Measuring Delaminations in Concrete Bridge Decks by Sounding, Tech. rep., ASTM International, West Conshohocken, PA (2012).
URL http://www.astm.org/cgi-bin/resolver.cgi?D4580D4580M-12

[7] S. K. U. Rehman, Z. Ibrahim, S. A. Memon, M. Jameel, Nondestructive test methods for concrete bridges: A review, Construction and Building Materials 107 (Supplement C) (2016) 58 – 86. doi:10.1016/j.conbuildmat.2015.12.011.
URL http://www.sciencedirect.com/science/article/pii/S0950061815306905

[8] R. Felicetti, Assessment of an industrial pavement via the impact acoustics method, European Journal of Environmental and Civil Engineering 14 (4) (2010) 427–439. doi:10.1080/19648189.2010.9693235.

[9] N. J. Carino, Training: Often the missing link in using NDT methods, Construction and Building Materials 38 (Supplement C) (2013) 1316 – 1329. doi:10.1016/j.conbuildmat.2011.03.060.
URL http://www.sciencedirect.com/science/article/pii/S0950061811001061

[10] ASTM C1383-15, Standard Test Method for Measuring the P-Wave Speed and the Thickness of Concrete Plates Using the Impact-Echo Method, Tech. rep., ASTM International, West Conshohocken, PA (2015).
URL http://www.astm.org/cgi-bin/resolver.cgi?C1383-15

[11] J. Zhu, J. S. Popovics, Imaging concrete structures using air-coupled impact-echo, Journal of Engineering Mechanics - ASCE 133 (6) (2007) 628–640. doi:10.1061/(ASCE)0733-9399(2007)133:6(628).

[12] Mary Sansalone, Nicholas J. Carino, Impact-Echo: A Method for Flaw Detection in Concrete Using Transient Stress Waves, Tech. Rep. NBSIR 86-3452, National Bureau of Standards (Sep. 1986).

[13] H. Haya, X. Luo, T. Inaba, T. Uomoto, Study on Impact Acoustic Method and System Development Based on Wavelet Analysis, in: Proceedings International Symposium Non-Destructive Testing in Civil Engineering (NDT-CE), Berlin, 2003.

[14] Arthur W. Leissa, Vibration of Plates, Technical Report NASA-SP-160, NASA, Washington, DC, United States (Jan. 1969).

[15] H. M. Nelson, High frequency flexural vibration of thick rectangular bars and plates, Journal of Sound and Vibration 60 (1) (1978) 101 – 118. doi:10.1016/0022-460X(78)90404-2.
URL http://www.sciencedirect.com/science/article/pii/0022460X78904042

[16] S. Hosseini-Hashemi, M. Eshaghi, H. R. D. Taher, M. Fadaie, Exact closed-form frequency equations for thick circular plates using a third-order shear deformation theory, Journal of Sound and Vibration 329 (16) (2010) 3382 – 3396. doi:10.1016/j.jsv.2010.02.024.
URL http://www.sciencedirect.com/science/article/pii/S0022460X10001471

[17] J. Lu, Advancements in evaluation of air-coupled impact-echo test method, Ph.D. thesis, Iowa State University, Ames, Iowa (2015).
URL http://lib.dr.iastate.edu/etd/14490

[18] M. Sansalone, W. Streett, Impact-echo: non-destructive evaluation of concrete and masonry, Bullbrier Press, 1997.

[19] A. Gudmarsson, N. Ryden, B. Birgisson, Non-contact excitation of fundamental resonance frequencies of an asphalt concrete specimen, AIP Conference Proceedings 1650 (1) (2015) 1401–1408. doi:10.1063/1.4914755.
URL http://aip.scitation.org/doi/abs/10.1063/1.4914755